



Cite this: *Phys. Chem. Chem. Phys.*,
2015, 17, 9942

Synthesis and hydrolysis of gas-phase lanthanide and actinide oxide nitrate complexes: a correspondence to trivalent metal ion redox potentials and ionization energies†

Ana F. Lucena,^a Célia Lourenço,^a Maria C. Michelini,^{*b} Philip X. Rutkowski,^c
José M. Carretas,^a Nicole Zorz,^d Laurence Berthon,^d Ana Dias,^e
M. Conceição Oliveira,^e John K. Gibson^c and Joaquim Marçalo^{*a}

Several lanthanide and actinide tetranitrate ions, $M^{III}(\text{NO}_3)_4^-$, were produced by electrospray ionization and subjected to collision induced dissociation in quadrupole ion trap mass spectrometers. The nature of the $\text{MO}(\text{NO}_3)_3^-$ products that result from NO_2 elimination was evaluated by measuring the relative hydrolysis rates under thermalized conditions. Based on the experimental results it is inferred that the hydrolysis rates relate to the intrinsic stability of the M^{IV} oxidation states, which correlate with both the solution IV/III reduction potentials and the fourth ionization energies. Density functional theory computations of the energetics of hydrolysis and atoms-in-molecules bonding analysis of representative oxide and hydroxide nitrates substantiate the interpretations. The results allow differentiation between those $\text{MO}(\text{NO}_3)_3^-$ that comprise an O^{2-} ligand with oxidation to M^{IV} and those that comprise a radical O^- ligand with retention of the M^{III} oxidation state. In the particular cases of $\text{MO}(\text{NO}_3)_3^-$ for $M = \text{Pr}, \text{Nd}$ and Tb it is proposed that the oxidation states are intermediate between $M^{(III)}$ and $M^{(IV)}$.

Received 27th January 2015,
Accepted 12th March 2015

DOI: 10.1039/c5cp00515a

www.rsc.org/pccp

Introduction

Thermal decomposition of metal nitrates to produce solid oxides is enabled by the susceptibility of NO_3 towards dissociation into NO_2 and O ($\Delta H_{289\text{K}}^0 = 211 \text{ kJ mol}^{-1}$),¹ a process that becomes favorable at high temperature when the NO_2 concentration in the vapor phase is low. Among the first reports of the thermal dissociation of solid metal nitrates was that by Butkow and Tschassowenny in 1936.² Several binary and ternary metal oxides have since been synthesized by nitrate decomposition,^{3–10}

including catalytic materials,^{11–13} thin films,^{14–16} and nanoparticles.^{17,18} Of particular relevance to the present work are reports of the decomposition of lanthanide nitrates.^{19–22} Dill and Meyer reported the partial decomposition of lanthanide nitrates, $\text{Ln}(\text{NO}_3)_3$, to produce novel oxide nitrate solids, $\text{LnO}(\text{NO}_3)$.²³

Decomposition of solid nitrates is a useful synthetic approach to novel materials. To understand fundamental aspects of the decomposition processes it is informative to study the fragmentation of elementary gas-phase species. Studies of the fragmentation of gas-phase metal nitrate anion complexes, $M(\text{NO}_3)_x^-$, have revealed the capability to induce changes in oxidation state: reduction by NO_3 elimination to produce $M(\text{NO}_3)_{x-1}^-$, or oxidation by NO_2 elimination to produce $\text{MO}(\text{NO}_3)_{x-1}^-$. Houk and co-workers employed electrospray ionization (ESI) of metal nitrate solutions to produce a variety of gas-phase metal nitrate anion complexes with metals having more than one stable oxidation state (e.g. $\text{Cu}^{\text{II}}/\text{Cu}^{\text{I}}$ and $\text{Fe}^{\text{III}}/\text{Fe}^{\text{II}}$) exhibiting both in the nitrate clusters.²⁴ This same group subsequently studied the fragmentation of these complexes by collision induced dissociation (CID).²⁵ The CID behavior of group I and II nitrates was rather straightforward, with loss of NO_3^- to produce $M^{\text{I}}(\text{NO}_3)$ for alkali metals, or $M^{\text{II}}(\text{NO}_3)_2$ for alkaline earth metals, results that reflect the inability to oxidize these metals. CID of Cu^{II} and Fe^{III} nitrate complexes resulted in NO_3 elimination concomitant with reduction to Cu^{I} and Fe^{II} . Several transition metal nitrate

^a Centro de Ciências e Tecnologias Nucleares, Instituto Superior Técnico, Universidade de Lisboa, 2695-066 Bobadela LRS, Portugal.
E-mail: jmarcalo@ctn.ist.utl.pt

^b Dipartimento di Chimica, Università della Calabria, 87030 Arcavacata di Rende, Italy. E-mail: mc.michelini@unical.it

^c Chemical Sciences Division, Lawrence Berkeley National Laboratory, Berkeley, CA 94720, USA

^d CEA, Nuclear Energy Division, Radiochemistry and Processes Department, Laboratory of Ligands-Actinides Interactions, 30207 Bagnols-sur-Cèze, France

^e Centro de Química Estrutural, Instituto Superior Técnico, Universidade de Lisboa, 1049-001 Lisboa, Portugal

† Electronic supplementary information (ESI) available: Complete reference 37. QTAIM topological properties of $M(\text{OH})(\text{NO}_3)_3^-$ and $\text{MO}(\text{NO}_3)_3^-$ complexes; $M = \text{La}, \text{Ce}, \text{Lu}, \text{Al}, \text{Sc}$, and Y . CID mass spectra of $\text{Ce}(\text{NO}_3)_4^-$, $\text{Tb}(\text{NO}_3)_4^-$, $\text{Tm}(\text{NO}_3)_4^-$, $\text{Sc}(\text{NO}_3)_4^-$, $\text{Y}(\text{NO}_3)_4^-$, $\text{Am}(\text{NO}_3)_4^-$. Kinetic plot for hydrolysis of $\text{HoO}(\text{NO}_3)_3^-$. See DOI: 10.1039/c5cp00515a

complexes eliminated NO_2 to produce $\text{MO}(\text{NO}_3)_{x-1}^-$.²⁵ For metal ions with prohibitively high ionization energies to achieve oxidation, such as Fe^{3+} ($\text{IE}[\text{Fe}^{3+}] = 54.8 \text{ eV}$),²⁶ it was reasonably concluded that the oxidation state is not increased in the oxide products.²⁵ In cases such as $\text{MnO}(\text{NO}_3)_2^-$ it is feasible that the elimination of NO_2 results in an increase in the oxidation state from Mn^{II} to Mn^{III} because $\text{IE}[\text{Mn}^{2+}] = 33.7 \text{ eV}$ is much lower.²⁶

Frański *et al.* recently reported on CID of transition metal nitrate anion clusters and concluded that elimination of NO_2 could result in extensive oxidation of the metals.²⁷ Among the oxidation states assigned were $\text{Mn}(\text{VII})$ in MnO_4^- , $\text{Cr}(\text{VI})$ in $\text{CrO}_3(\text{NO}_3)^-$, $\text{Fe}(\text{VI})$ in $\text{FeO}_3(\text{NO}_3)^-$, and $\text{Co}(\text{V})$ in CoO_3^- . There was no direct evidence for these assignments; the structures of the gas-phase oxides were assumed to comprise only $\text{M}=\text{O}$ bonds in which formal charge state is O^{2-} . In gas-phase metal complexes that have multiple ligating oxygen atoms it is well established that peroxy (O_2^{2-}) and superoxy (O_2^-) are stable ligands, such as in $[\text{U}^{\text{VI}}\text{O}_2(\text{O}_2)]^+$.²⁸ Li *et al.* have computed that the ground state of plutonium tetroxide is not $\text{Pu}^{\text{VIII}}\text{O}_4$ but is rather the superoxide $\text{Pu}^{\text{VO}}\text{O}_2(\text{O}_2^-)$ in which Pu is remarkably not even in its readily accessible hexavalent oxidation state as it would be in the peroxide $\text{Pu}^{\text{VI}}\text{O}_2(\text{O}_2^{2-})$.²⁹ It is apparent that the assumption that all oxygen atoms in metal oxide clusters can be considered as O^{2-} is not well founded. This issue was addressed by Groenewold *et al.*, who concluded that NO_2 loss from $\text{U}^{\text{VI}}\text{O}_2(\text{NO}_3)_3^-$ induced by infrared multiphoton dissociation (IRMPD) produced $\text{U}^{\text{VI}}\text{O}_2(\text{NO}_3)_2(\text{O})^-$ in which the additional oxygen ligand is an O^- radical.³⁰ In that same work, IRMPD of $\text{Eu}(\text{NO}_3)_4^-$ resulted in NO_3 loss and NO_2 loss (as well as additional channels). The $\text{Eu}(\text{NO}_3)_3^-$ product almost certainly comprises the stable $\text{Eu}(\text{II})$ oxidation state but the nature of the oxygen ligand and the europium oxidation state in $\text{EuO}(\text{NO}_3)_3^-$ is not obvious. The variable nature of the oxygen ligand in metal oxide nitrates such as this is further addressed in the present work. In an IRMPD study of $\text{M}^{\text{II}}(\text{NO}_3)_3^-$, where M is an alkaline earth metal, the observed dissociation channel was NO_3^- elimination to produce neutral $\text{M}^{\text{II}}(\text{NO}_3)_2$ in which the divalent oxidation state is retained.³¹ CID of cobalt and nickel nitrate cation clusters studied by Schröder *et al.* resulted in the loss of NO_2 to result in oxide species with reasonable modest oxidation states.³² In other work, Schröder *et al.* prepared (phenanthroline) $\text{Cu}^{\text{III}}\text{O}^+$ by CID-induced NO_2 -elimination from (phenanthroline) $\text{Cu}^{\text{II}}(\text{NO}_3)^+$.³³

In the work reported here several $\text{M}^{\text{III}}(\text{NO}_3)_4^-$ were produced by ESI and subjected to low-energy CID in quadrupole ion trap mass spectrometers (QIT-MS). The nature of the $\text{MO}(\text{NO}_3)_3^-$ products that result from NO_2 elimination was experimentally evaluated by their hydrolysis to produce $\text{M}^{\text{III}}(\text{OH})(\text{NO}_3)_3^-$. Density functional theory (DFT) computations of the structure and bonding of representative nitrate precursors, oxide and hydroxide nitrates, as well as the energetics of hydrolysis provide insights into the experimental results and allow differentiation between those $\text{MO}(\text{NO}_3)_3^-$ that comprise an O^{2-} ligand with oxidation to M^{IV} , and those that comprise an O^- ligand with retention of the M^{III} oxidation state.

Experimental approach

The ^{242}Pu , ^{241}Am and ^{248}Cm isotopes used in this work are alpha-emitting radionuclides with half-lives of 4×10^5 years, 433 years and 3×10^5 years, respectively. Special safety precautions must be followed when handling these isotopes. The experiments reported here with these radionuclides were performed in special radiological containment glove boxes.

The QIT-MS experiments were performed using four instruments, each equipped with ESI interfaces with MS^n CID capabilities: a Bruker HCT at Centro de Ciências e Tecnologias Nucleares, Instituto Superior Técnico, Portugal (C2TN), a Varian 500-MS IT at Centro de Química Estrutural, Instituto Superior Técnico, Portugal (CQE), a Bruker Esquire-LC at CEA-Marcoule, France (CEA), and an Agilent 6340 at Lawrence Berkeley National Laboratory, USA (LBNL). The instruments at C2TN and CQE allowed comparison of results for widely divergent background water pressures. The instruments at CEA and LBNL enabled the study of highly radioactive actinides Pu, Am and Cm.

Solutions of $\text{Ln}^{\text{III}}(\text{NO}_3)_3(\text{H}_2\text{O})_x$ and $\text{An}(\text{III})$ were prepared in water, ethanol or isopropanol with most concentrations in the range 10^{-3} to 10^{-4} M; the concentration of $\text{Cm}(\text{III})$ was less than 10^{-5} M. $\text{Am}(\text{NO}_3)_3$ solutions of 10^{-4} M in ethanol and in water were prepared from the stock solution of 1.5×10^{-3} M $\text{Am}(\text{NO}_3)_3$ with a HNO_3 concentration of 0.1 M. Pu-242 and Cm-248 nitrate stock solutions were diluted to prepare 1.8×10^{-4} M and 5×10^{-6} M solutions, respectively, for ESI.

All four instruments were operated in the negative ion accumulation and detection mode. The metal nitrate solutions were directly injected into the capillaries in the ESI sources using syringe pumps with flow rates in the range of 60–600 $\mu\text{L h}^{-1}$.

For the Bruker HCT at C2TN, sample solutions were introduced with a flow rate of 150 $\mu\text{L h}^{-1}$. The spectra were acquired using the following typical instrumental parameters: capillary voltage 4000 V, nebulizer gas (N_2) pressure 8.0 psi, drying gas (N_2) at 250 °C with flow rate 4.0 L min^{-1} , capillary exit voltage -128.5 V, skimmer voltage -40.0 V, trap drive 67.3 V.

For the Varian 500-MS IT at CQE spectra were acquired using the following instrumental parameters: solution flow rate 600 $\mu\text{L h}^{-1}$, capillary voltage -20 V, needle -4500 V, spray shield -600 V, radiofrequency (RF) load 90%, nebulizer gas (N_2) pressure 35 psi, drying gas (N_2) pressure 10 psi at 350 °C.

The Bruker Esquire-LC at CEA was installed in a radiological-containment glove box.³⁴ A syringe infusion pump delivered the sample at 90 $\mu\text{L h}^{-1}$ to the electrospray source. The experimental conditions were the following: drying gas (N_2) 5 L min^{-1} at 250 °C, nebulizer gas (N_2) pressure 5 psi, ion spray voltage 4000 V, capillary exit offset -60 V, skimmer (1) -60 V, skimmer (2) -10 V, trap drive 50 V.

The Agilent 6340 QIT/MS (LBNL), which is essentially the same as the Bruker HCT, was operated also with the source region of the QIT/MS inside of a radiological-containment glove box, as previously described.³⁵ Spectra were typically acquired using the following approximate instrumental parameters: solution flow rate 60 $\mu\text{L h}^{-1}$, nebulizer gas (N_2) 15 psi, capillary voltage 4500 V and current 15 nA, dry gas (N_2 from a boil-off of a liquid

nitrogen Dewar) flow rate 5 L min^{-1} at $325 \text{ }^\circ\text{C}$, capillary exit -160 V , skimmer -50 V , trap drive 140 V . As has been discussed elsewhere,³⁶ the background water pressure in this ion trap is estimated as $\sim 10^{-6} \text{ Torr}$.

The buffer gas used in the four ion traps was helium (constant pressure of $\sim 1 \times 10^{-4} \text{ mbar}$). Ion/molecule reactions can occur in the ion trap by applying a variable reaction delay time of up to 10 s at the trap temperature of $\sim 300 \text{ K}$.³⁷ Collision induced dissociation (CID) experiments are performed by isolation of the ions of interest and ejection of all the other ions, which allows time-dependent hydration reaction studies with the background water in the traps under thermal conditions. Because the CID and other instrumental conditions were not identical for all four instruments, comparisons between CID product yields are necessarily somewhat qualitative. Relative hydration rates were measured under low-energy thermal conditions such that they can be directly compared, with differences in rates attributable to different background water pressures in the ion traps.

Pseudo-first order reaction rates, k , for thermal (*ca.* 300 K) hydrolysis of trapped ions in the QITs were obtained by isolating the ion of interest and allowing it to react with background water for variable times. Plots of the logarithmic decay of the ratio of the reactant ion intensity to the total ion intensity as a function of time provide the hydrolysis reaction rates. The hydrolysis rates were different for the four QITs due to different water pressures, by up to a factor of 100 times, in the ion traps. As described below, by obtaining rates for the same hydrolysis reaction in all four QITs (for $\text{ScO}(\text{NO}_3)_3^-$) it was possible to establish the following relative water pressures (arbitrarily normalized to 100 for the C2TN trap): C2TN/100; LBNL/62; CEA/8.6; CQE/1.3. As remarked above, the C2TN and LBNL instruments are essentially identical; the lower water pressure in the LBNL trap might be due to the use of high-purity N_2 evaporated from liquid nitrogen, rather than from a nitrogen generator.

Computational methods

DFT computations of the structure of representative nitrate precursors, oxide nitrates and hydroxide nitrates were performed using the Gaussian09 (revision B.01) package.³⁸ Full geometry optimizations and frequency calculations were performed using the B3LYP hybrid functional.^{39,40} The Stuttgart-Dresden triple- ζ valence basis sets together with the corresponding effective small-core potential (SDD) were used for the lanthanide and transition metal (Sc,Y) atoms^{41,42} and the Pople triple- ζ basis sets, 6-311++G(d,p), for the rest of the atoms.^{43–45} The “ultrafine” pruned grid was adopted for the numerical integration option in all computations. Geometry optimizations were performed without symmetry restrictions. Computation of open-shell systems were performed using spin-unrestricted methods. The broken-symmetry (BS) approach^{46–49} was used to study the open-shell $\text{CeO}(\text{NO}_3)_3^-$ (singlet spin state) and the antiferromagnetically coupled $\text{PrO}(\text{NO}_3)_4^-$ (doublet spin state). All the computed reaction energies include the zero-point vibrational energy correction (ΔE^0). In addition to the ΔE^0 values, the Gibbs free energy at 298 K is

reported for each of the studied reactions (ΔG^{298}). The accuracy of the ΔG^{298} values is necessarily somewhat limited by the use of the harmonic oscillator approximation to treat nuclear motion. It should be remarked that all of the computations were performed for a pressure of 1 atm . In reality, the total pressure under these experimental conditions is approximately 10^{-4} Torr . Furthermore, the “pressures” of the reactants and products, both ions and neutrals, are very low ($\leq 10^{-6} \text{ Torr}$) and are unknown. Accordingly, the computed reaction entropies and free energies may deviate from the actual values under these experimental conditions. However, the values for ΔE^0 are not pressure dependent and the key conclusions, which are based on ΔE^0 values, are not affected by the uncertainties in ΔG^{298} . QTAIM analysis⁵⁰ was performed on all the studied $\text{MO}(\text{NO}_3)_4^-$ and $\text{M}(\text{OH})(\text{NO}_3)_3^-$ complexes to analyze and compare the characteristics of the M–O bonds. Appropriate wavefunction extended files (wfx) were obtained with Gaussian09 and analyzed using the AIMAll package.⁵¹ The electron density (ρ_{BCP}), the Laplacian of electron density ($\nabla^2 \rho_{\text{BCP}}$) and total energy density (H_{BCP}) of the M–OH and M–O (oxide) bond critical point of the $\text{M}(\text{OH})(\text{NO}_3)_3^-$ and $\text{MO}(\text{NO}_3)_3^-$ complexes (M = La, Ce, Pr, Lu, Al, Sc, and Y) are included as ESI† (Table S1).

Results and discussion

The first experimental component of this work was a study of the fragmentation behavior of $\text{M}^{\text{III}}(\text{NO}_3)_4^-$ complexes, with an emphasis on how the product distributions relate to the intrinsic stability of the M(IV) oxidation states. The second part involved studying the kinetics of hydrolysis of fragmentation products to produce M(III) hydroxides. The experimental observations are evaluated in comparison with computed structures of the products, and the computed energetics of the fragmentation and hydrolysis processes.

Fragmentation of $\text{M}(\text{NO}_3)_4^-$

The key CID results for the $\text{M}(\text{NO}_3)_4^-$ complexes are in Table 1. The dominant products were $\text{MO}(\text{NO}_3)_3^-$ and $\text{M}(\text{OH})(\text{NO}_3)_3^-$ (representative CID mass spectra are in ESI†). For several of the $\text{M}(\text{NO}_3)_4^-$ an additional minor ($< 10\%$) product was $\text{MO}_2(\text{NO}_3)_3^-$ *via* elimination of NO, but the nature of these species and other secondary products (see ESI†) are not considered in detail here, except to mention that the $\text{MO}_2(\text{NO}_3)_3^-$ may be superoxides comprising an O_2^- ligand, such that the stable M(III) oxidation state is retained. In the distinctive cases of $\text{Eu}(\text{NO}_3)_4^-$ and $\text{Yb}(\text{NO}_3)_4^-$, a very minor ($\leq 5\%$) CID channel was ligand loss to produce $\text{M}(\text{NO}_3)_3^-$ in which the metal has been reduced from a formal M(III) to a M(II) oxidation state. Previous work has demonstrated that CID of gas-phase complexes parallels solution redox chemistry, with metal complexes having higher reduction potentials being more prone to reduction upon CID.⁵² The observed reduction of Eu(III) and Yb(III) to the divalent state by ligand loss is consistent that these two are the studied M(III) with the less negative III/II reduction potentials.⁵³

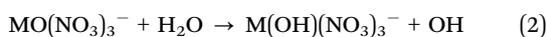
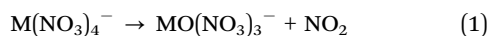
The dominant CID process is given by eqn (1). The appearance of substantial hydroxide suggests that eqn (2) occurs

Table 1 Product yields for CID of $M(\text{NO}_3)_4^-$ ^a

	$\text{MO}(\text{NO}_3)_3^-$	$\text{M}(\text{OH})(\text{NO}_3)_3^-$
La	5/45	85/50
Ce	100/100	0/0
Pr	100/100	0/0
Nd	100/100	0/0
Sm	<3/55	95/40
Eu ^b	0/45	95/45
Gd	10/50	90/50
Tb	100/100	0/0
Dy	10/55	85/45
Ho	10/60	90/40
Er	5/60	90/40
Tm	10/60	90/40
Yb ^b	<3/60	95/35
Lu	10/50	80/50
Sc	55/100/70 ^c	45/0/25 ^c
Y	10/55	90/40
Al	100	0
Pu	95 ^c	0 ^c
Am	100 ^d	0 ^d
Cm	100 ^c	0 ^c

^a Intensities of product ions, rounded to 5% to reflect reproducibility. Where two values are given, that in regular font (left) if from CT2N and that in italics (right) is from CQE. A value of <3% indicates detection in the range of 1–2%; 0% indicates not detected to <1%. Small (<10%) yields of $\text{MO}_2(\text{NO}_3)_3^-$ were observed, except for M = Ce, Pr, Eu, Al and Cm. ^b $\text{M}(\text{NO}_3)_3^-$ was produced at ~5% yield for M = Eu and at ~1% yield for M = Yb. ^c From LBNL. ^d From CEA.

efficiently under CID conditions as a secondary reaction. The efficiency of eqn (2) depends on both the background water pressure in the ion trap and the nature of the reactant ion. An alternative source of $\text{M}(\text{OH})(\text{NO}_3)_3^-$ is direct hydrolysis of the nitrate, eqn (3).



Structures of representative $\text{M}(\text{NO}_3)_4^-$, $\text{MO}(\text{NO}_3)_3^-$ and $\text{M}(\text{OH})(\text{NO}_3)_3^-$ shown in Fig. 1, with key M–O bond distances given in Table 2, are discussed below. Computed energetics for eqn (1)–(3) are in Table 3. Eqn (3) can be excluded as a significant pathway based on the following considerations. Eqn (3) involves no change in oxidation state and corresponds to the replacement of a nitrate ligand by a hydroxide ligand concomitant with consumption of H_2O and elimination of HNO_3 . Although there may be minor variations in the kinetics and thermodynamics associated with such a process across the lanthanide series, there is no basis to expect the observed substantial differences in hydroxide yields, particularly for adjacent lanthanides. For example, the result that under essentially the same conditions substantial $\text{La}^{\text{III}}(\text{OH})(\text{NO}_3)_3^-$ is produced whereas no $\text{Ce}^{\text{III}}(\text{OH})(\text{NO}_3)_3^-$ is produced (Table 1) indicates that eqn (3) is not a significant source of the $\text{M}^{\text{III}}(\text{OH})(\text{NO}_3)_3^-$ products. This interpretation is substantiated by the computed energetics for eqn (3) (Table 3), which indicate that both ΔE^0 and ΔG^{298} are essentially the same for M = La, Ce, Pr and Lu.

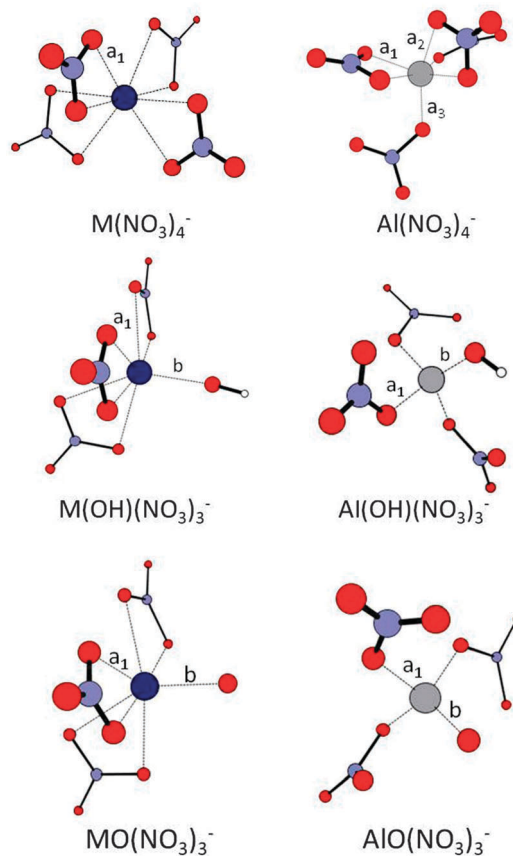


Fig. 1 Geometrical structures of ground state $\text{Al}(\text{NO}_3)_4^-$, $\text{Al}(\text{OH})(\text{NO}_3)_3^-$, $\text{AlO}(\text{NO}_3)_3^-$ ions, and of ground state $\text{M}(\text{NO}_3)_4^-$, $\text{M}(\text{OH})(\text{NO}_3)_3^-$, $\text{MO}(\text{NO}_3)_3^-$ ions for M = La, Ce, Pr, Sc, Y and Lu. Selected geometrical parameters are reported in Table 2.

Table 2 Selected optimized M–O bond distances^a

M	$\text{M}(\text{NO}_3)_4^-$ a_1, a_2, a_3	$\text{M}(\text{OH})(\text{NO}_3)_3^-$ $a_1; b$	$\text{MO}(\text{NO}_3)_3^-$ $a_1; b$
La	2.56 [8]	2.60 [6]; 2.15	2.59 [6]; 2.26
Ce	2.54 [8]	2.58 [6]; 2.13	2.55 [6]; 1.80
Pr	2.52 [8]	2.56 [6]; 2.06	2.54 [6]; 1.85
Lu	2.34 [8]	2.37 [6]; 2.00	2.36 [6]; 2.09
Al ^b	1.95 [2], 2.03 [2]; 1.85 [2]	1.84 [3]; 1.72	1.84 [3]; 1.77
Sc	2.23 [8]	2.26 [6]; 1.89	2.25 [6]; 1.96
Y	2.40 [8]	2.43 [6]; 2.05	2.42 [6]; 2.16

^a In Angstroms (see Fig. 1); values of a_1, a_2 and a_3 are averaged values over the number of nearly equivalent (to within ~0.01 Å) coordinating oxygen atoms in the NO_3 ligands, with the number of M–O interactions indicated in brackets. ^b $\text{Al}(\text{NO}_3)_4^-$ presents three sets of values, a_1 and a_2 for the two bidentate nitrates, and the shorter a_3 distance for the two monodentate nitrates (see Fig. 1). Al–O distances of >2.8 Å for $\text{Al}(\text{OH})(\text{NO}_3)_3^-$ and $\text{AlO}(\text{NO}_3)_3^-$ are not reported.

The results in Table 1 were acquired using four different QITs with widely disparate background water pressures. The CID results for $\text{Ln}(\text{NO}_3)_4^-$ are reported for the C2TN and CEA ion traps; the water pressure is *ca.* 100 times lower in the latter (see below). It is apparent that the yields of $\text{Ln}(\text{OH})(\text{NO}_3)_3^-$ by eqn (2) are substantially greater in the C2TN ion trap. A typical CID duration is *ca.* 40 ms, which is sufficient time for significant hydrolysis.

Table 3 Computed energetics (kJ mol^{-1}) for formation of $\text{MO}(\text{NO}_3)_3^-$ by elimination of NO_2 from $\text{M}(\text{NO}_3)_4^-$ (eqn (1)), for hydrolysis of $\text{MO}(\text{NO}_3)_3^-$ to form $\text{M}(\text{OH})(\text{NO}_3)_3^-$ (eqn (2)), and for hydrolysis of $\text{M}(\text{NO}_3)_4^-$ to form $\text{M}(\text{OH})(\text{NO}_3)_3^-$ (eqn (3))

	Eqn (1)		Eqn (2)		Eqn (3)	
	ΔE^0	ΔG^{298}	ΔE^0	ΔG^{298}	ΔE^0	ΔG^{298}
La	287	235	-17	-12	96	86
Ce	177	137	93	88	95	85
Pr	261	216	10	6	96	85
Lu	282	229	-13	-10	95	83
Sc	262	207	-7	-5	80	66
Y	289	236	-16	-12	98	88
Al	223	164	-10	-7	38	21

Among the lanthanide nitrates, $\text{LnO}(\text{NO}_3)_3^-$ was the sole product only in the cases of $\text{Ln} = \text{Ce}, \text{Pr}, \text{Nd}, \text{Tb}$ (Table 1). As is evident in Table 4, these are the four Ln with the lowest fourth ionization energies (IE4) and also the lowest IV/III reduction potentials. The IV/III reduction potentials are related to IE4 and are only estimates except for the case of $\text{Ce}(\text{IV/III})$.⁵³ Whereas reduction potentials are most pertinent in solution, ionization energies are most relevant in gas phase where solvation does not play a role. Accordingly, the remainder of the discussion will focus on comparative ionization energies, specifically IE4, with the understanding that there is a correlation to IV/III reduction potentials. The correlation between IE4 and abundance suggests that the stability of the $\text{LnO}(\text{NO}_3)_3^-$ ions are directly related to the stability of Ln^{4+} , and that the four $\text{LnO}(\text{NO}_3)_3^-$ produced exclusively upon CID can be considered as nitrate-coordinated lanthanide monoxides in which the oxidation state is $\text{Ln}(\text{IV})$ or intermediate between $\text{Ln}(\text{III})$ and $\text{Ln}(\text{IV})$. The computational results below confirm that the oxidation state is $\text{Ce}(\text{IV})$ in $\text{CeO}(\text{NO}_3)_3^-$.

Table 4 Selected properties of metal ions

	$\text{IE}[\text{M}^{3+} \rightarrow \text{M}^{4+}]^a$ (eV)	$\Delta E[\text{IV/III}]^b$ (V)	$r[\text{M}^{3+}]^c$ (Å)
La	50.0	—	1.06
Ce	36.8	+1.7	1.03
Pr	39.0	+3.7	1.01
Nd	40.4	+4.9	1.00
Sm	41.4	+5.5	0.96
Eu	42.7	+6.6	0.95
Gd	44.0	+7.9	0.94
Tb	39.8	+3.3	0.92
Dy	41.5	+4.9	0.91
Ho	42.5	+5.9	0.89
Er	42.7	+6.0	0.88
Tm	42.7	+6.0	0.87
Yb	43.6	+6.9	0.86
Lu	45.3	+8.5	0.85
Sc	73.5	—	0.73
Y	60.6	—	0.89
Al	120.0	—	0.53
Pu	34.6	+1.1	1.00
Am	36.2	+2.6	1.01
Cm	36.8	+3.0	0.98

^a Fourth ionization energies from ref. 26; values for Pu, Am and Cm are estimates from ref. 54. ^b IV/III reduction potentials. Values for $\text{Ln}(\text{IV/III})$ are from ref. 53; all except for Ce are estimates. Values for $\text{An}(\text{IV/III})$ are from ref. 55. Values not provided are predicted to be $\gg 10$ V. ^c Effective ionic radii from Shannon and Prewitt for CN6.⁵⁶

For CID of the other ten $\text{Ln}(\text{NO}_3)_4^-$ there is a significant amount of $\text{Ln}(\text{OH})(\text{NO}_3)_3^-$. According to our computations and bonding analysis (see below), the lanthanide atoms in $\text{LnO}(\text{NO}_3)_3^-$ and $\text{Ln}(\text{OH})(\text{NO}_3)_3^-$ ($\text{Ln} = \text{La}, \text{Lu}$) are Ln^{3+} coordinated by a radical oxygen or a hydroxide and three nitrate anion ligands. As there is no change in oxidation state, the yields of the $\text{Ln}(\text{OH})(\text{NO}_3)_3^-$ are similar for different Ln, 80–95% at C2TN and 35–50% at CQE, with no correlation of the hydroxide yields with IE4.

Three actinide nitrates were subjected to CID for comparison with the lanthanides. CID of $\text{An}(\text{NO}_3)_4^-$ for $\text{An} = \text{Pu}, \text{Am}$ and Cm resulted in $\text{AnO}(\text{NO}_3)_3^-$, with no detected $\text{An}(\text{OH})(\text{NO}_3)_3^-$. As seen in Table 4, IE4 of Pu, Am and Cm are less than or equal to IE4[Ce], suggesting that the three $\text{AnO}(\text{NO}_3)_3^-$ comprise $\text{An}(\text{IV})$.

To elucidate the role of ionic radii on hydrolysis, CID of $\text{M}(\text{NO}_3)_4^-$ for $\text{M} = \text{Sc}, \text{Y}$ and Al was studied, with the results in Table 1. Based on the very high IE4 values of these metals (Table 4) it can be confidently predicted that these are $\text{M}(\text{III})$ oxides and from the Ln results that hydrolysis should be prevalent as in the case of $\text{Y}(\text{NO}_3)_4^-$. For $\text{Sc}(\text{NO}_3)_4^-$, the yield of $\text{ScO}(\text{NO}_3)_3^-$ is higher, 100% at CQE, than would be predicted from the high IE4 for Sc. For $\text{Al}(\text{NO}_3)_4^-$, only $\text{AlO}(\text{NO}_3)_3^-$ was produced, with no evidence for hydrolysis, which is remarkable in view of the very high Al IE4 of 120 eV. As is seen in Table 4, the ionic radius of Y^{3+} is comparable to those of the late Ln^{3+} whereas that of Sc^{3+} is 0.12 Å smaller than that of Lu^{3+} and that of Al^{3+} is 0.33 smaller than that of Lu^{3+} . It is inferred that $\text{MO}(\text{NO}_3)_3^-$ having M^{3+} with sufficiently small radii are resistant to hydrolysis under CID conditions regardless of the magnitude of IE4.

Hydrolysis of $\text{MO}(\text{NO}_3)_3^-$

To study hydrolysis under thermal conditions for comparison with the CID results, rates for eqn (2) were measured for $\text{MO}(\text{NO}_3)_3^-$, with the results compiled in Table 5 for the four different QIT mass spectrometers. The measured pseudo-first order rates for eqn (3) were obtained from the decay of the reactant according to eqn (4).

$$-d[\text{MO}(\text{NO}_3)_3^-]/dt \equiv \text{rate} = k_{\text{M}}[\text{H}_2\text{O}] \quad (4)$$

An example of data for $\text{ScO}(\text{NO}_3)_3^-$ used to obtain hydrolysis rates is shown in Fig. 2 with the corresponding kinetics plot in Fig. 3. Hydrolysis rates were measured for $\text{ScO}(\text{NO}_3)_3^-$ in all four QITs (Table 5). Because the rate constant, k_{Sc} , is invariant, the relative rates provide the relative water pressure, $[\text{H}_2\text{O}]$, in the traps (normalized to 100 at C2TN): C2TN/100; LBNL/62; CEA/8.6; CQE/1.3. The invariance of the water pressures in each trap, to within ca. 10%, was confirmed by establishing that the measured rates did not vary significantly when measured at different times. It has been estimated that the water pressure in the LBNL ion trap is ca. 10^{-6} Torr; the pressure in the C2TN trap is roughly comparable, that in the CEA trap significantly lower, and that in CQE trap is even lower.

The predicted resistance of tetranitrates, $\text{M}(\text{NO}_3)_4^-$, towards spontaneous hydrolysis according to eqn (3) was confirmed for $\text{M} = \text{La}, \text{Tb}, \text{Eu}, \text{Ho}, \text{Lu}, \text{Sc}, \text{Y}, \text{Al}$ and Pu . The $\text{M}(\text{NO}_3)_4^-$ were isolated in either the C2TN or LBNL traps, which have the

Table 5 Hydrolysis rates for $\text{MO}(\text{NO}_3)_3^-$ ^a

	k (s^{-1})
La	7.0
Ce	NR/NR
Pr	NR ^b /NR
Nd	0.012/NR
Sm	5.3
Eu	5.0
Gd	5.6
Tb	0.006/NR
Dy	5.3
Ho	5.5
Er	5.3
Tm	5.7
Yb	4.7
Lu	5.5
Sc	10.4/0.13/0.89 ^c /6.4 ^d
Y	6.5
Al	0.15
Pu	NR ^d
Am	NR ^c
Cm	NR ^d

^a Unless otherwise noted the values in regular font were obtained at C2TN and those in italics at CQE; the results for Pu and Cm were obtained at LBNL, and those for Am at CEA. NR means no reaction for the 10 s maximum reaction time. Most of the Ln and Y hydrolyzed too rapidly in the C2TN instrument to allow isolation and rate determinations. ^b Increasing the water pressure in the C2TN trap by a factor of ca. 5× resulted in minuscule but detectable hydration. Normalization to the usual background pressure in the trap results in an estimated rate of 0.0001 s^{-1} , ca. 60× slower than the rate for $\text{TbO}(\text{NO}_3)_3^-$. ^c Measured at CEA. ^d Measured at LBNL.

highest water pressures, with a 10 s reaction time applied: there was no indication of any $\text{M}(\text{OH})(\text{NO}_3)_3^-$ products.

All of the $\text{LnO}(\text{NO}_3)_3^-$, as well as $\text{ScO}(\text{NO}_3)_3^-$ could be isolated in the CQE ion trap for determination of hydrolysis rates. For Ln = Ce, Pr, Nd and Tb, no hydrolysis was observed after isolation for the maximum accessible reaction time of 10 s. For all other Ln, the hydrolysis rates were similar, in the narrow range of 5–7 s^{-1} . The rate for $\text{ScO}(\text{NO}_3)_3^-$, 0.13 s^{-1} , was notably slower. The $\text{MO}(\text{NO}_3)_3^-$ complexes could be isolated and hydrolysis rates obtained in the C2TN trap for M = Ce, Pr, Nd, Tb, Sc, and Al. There was no detectable hydrolysis for M = Ce and Pr after the maximum reaction time of 10 s. By increasing the water pressure by a factor of five, very inefficient hydrolysis of $\text{PrO}(\text{NO}_3)_3^-$ (but not $\text{CeO}(\text{NO}_3)_3^-$) could be detected, as noted in Table 5; this very inefficient process could be attributed to a small population of non-thermalized ions. The measured rates for Nd and Tb, 0.012 s^{-1} and 0.006 s^{-1} , respectively were much slower than for M = Sc (10.4 s^{-1}) and Al (0.15 s^{-1}). The results that $\text{CeO}(\text{NO}_3)_3^-$ and $\text{PrO}(\text{NO}_3)_3^-$ do not spontaneously hydrolyze is consistent with the computed energetics for eqn (2) in Table 3. The computations predict that $\text{MO}(\text{NO}_3)_3^-$ for M = La, Lu, Sc, and Al should spontaneously hydrolyze, as experimentally observed, with the slower rates for the latter two attributed to the small ionic radii of Sc^{3+} and Al^{3+} . The computed exothermicities for those $\text{MO}(\text{NO}_3)_3^-$ that do hydrolyze differ by 10 kJ mol^{-1} or less; for oxides that can be considered as $\text{Ln}^{\text{III}}\text{O}(\text{NO}_3)_3^-$, the oxidation state of the metal does not change upon hydrolysis and similar rates are thus expected.

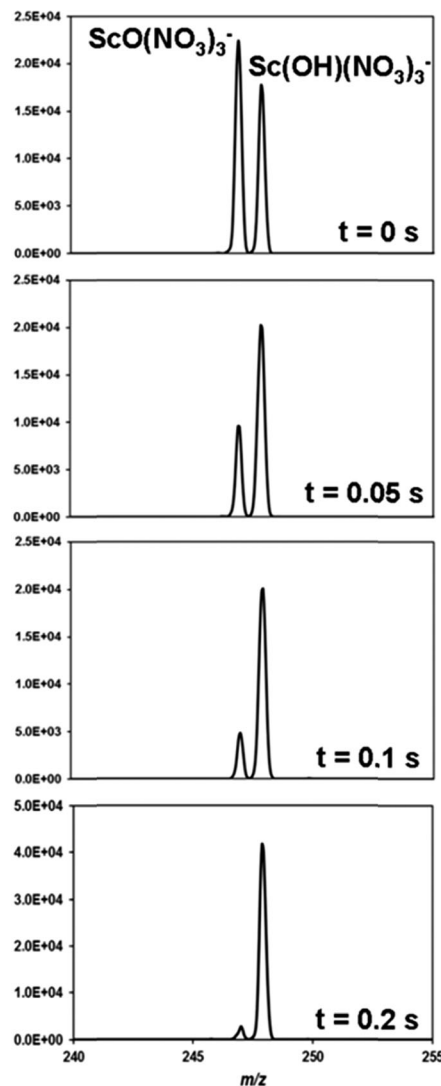


Fig. 2 Hydrolysis of $\text{ScO}(\text{NO}_3)_3^-$ as observed at C2TN. The indicated time is the delay between isolation of $\text{ScO}(\text{NO}_3)_3^-$ and detection of the residual reactant and hydrolysis product; the appearance of substantial product for $t = 0 \text{ s}$ is a result of the ca. 0.04 s time for isolation.

Computed structures and bonding analysis of the nitrate complexes

For M = La, Ce, Pr, Lu, Sc and Y, the computed ground state structures of $\text{M}(\text{NO}_3)_4^-$, $\text{MO}(\text{NO}_3)_3^-$ and $\text{M}(\text{OH})(\text{NO}_3)_3^-$ are shown in Fig. 1 with the M–O distances given in Table 2. In the $\text{Ln}(\text{NO}_3)_4^-$ the four nitrates exhibit bidentate coordination with the Ln–O bond lengths contracting from La to Lu in accord with the lanthanide contraction. The Ln–O distances decrease by 0.22 Å from $\text{La}(\text{NO}_3)_4^-$ to $\text{Lu}(\text{NO}_3)_4^-$ (Table 2); the ionic radii decrease by 0.21 Å from La^{3+} to Lu^{3+} (Table 4). The $\text{Ln}(\text{OH})(\text{NO}_3)_3^-$ (Fig. 1) have three bidentate nitrate ligands and one hydroxide ligand, with the decrease in Ln–OH bond distances from La to Lu of 0.15 Å again in accord with the lanthanide contraction. It is apparent that the $\text{Ln}(\text{NO}_3)_4^-$ and $\text{Ln}(\text{OH})(\text{NO}_3)_3^-$ are Ln(III) complexes, which was verified by QTAIM bond analysis. La and Lu hydroxides are in their singlet

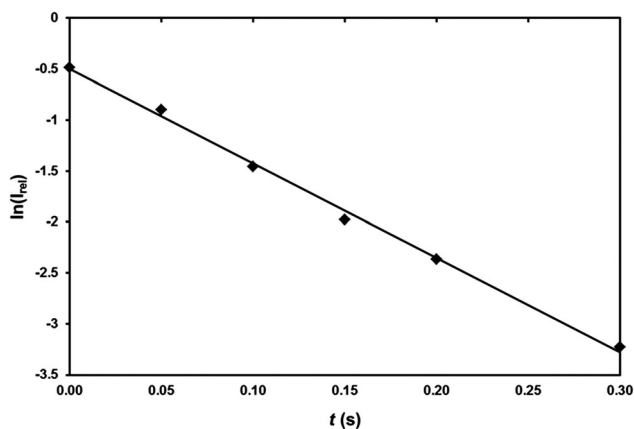


Fig. 3 Kinetic plot from the reaction of isolated $\text{ScO}(\text{NO}_3)_3^-$ with H_2O to form $\text{Sc}(\text{OH})(\text{NO}_3)_3^-$ from results obtained at C2TN ($R^2 = 0.9967$).

ground spin state, whereas in $\text{Ce}(\text{OH})(\text{NO}_3)_4^-$ (doublet spin state) and $\text{Pr}(\text{OH})(\text{NO}_3)_4^-$ (triplet spin state) the spin density is localized on the metal atoms. The topological properties concerning the M–OH bonds of the $\text{Ln}(\text{OH})(\text{NO}_3)_4^-$ complexes are summarized in Table S1 (ESI[†]). All hydroxides show electron densities at the M–OH bond critical points (ρ_{BCP}) that are close to 0.10 a.u., the Laplacian of the electron density at the BCPs, $\nabla^2\rho_{\text{BCP}}$, are positive, and the total electronic energy densities (H_{BCP}) values are very small and negative (between -0.0064 and -0.0237 a.u.). M–OH topological properties are comparable with the corresponding M–O (nitrates) ρ_{BCP} values, indicating a similar type of interaction. The delocalization indexes (DI) indicate that in all cases the number of electrons shared by the metal and oxygen atoms is very low (<0.75 e). In all cases the metal electronic configuration of the $\text{M}(\text{OH})(\text{NO}_3)_4^-$ ions is consistent with the Ln(III) oxidation state, and the bonding topologies characteristic of closed-shell interactions (*i.e.* ionic bonds).

The nature of the $\text{LnO}(\text{NO}_3)_3^-$ complexes is quite more intriguing in view of the variable IE4 and stabilities of the Ln(IV) oxidation states. The structures of the $\text{LnO}(\text{NO}_3)_3^-$ are similar, with three bidentate nitrates and one Ln–O linkage. The decrease in the Ln–O nitrate distance, 0.23 Å from La to Lu, is again indicative of ionic bonding to the metal centers. The clear distinction between the structures of the $\text{LnO}(\text{NO}_3)_3^-$ is that the Ln–O (oxide) distance does not whatsoever correspond to the lanthanide contraction. For $\text{CeO}(\text{NO}_3)_3^-$ (singlet spin state) the Ce–O distance is 0.33 Å shorter than the Ce–OH distance in $\text{Ce}(\text{OH})(\text{NO}_3)_3^-$, indicating significant double bond character and a Ce(IV) oxidation state in the oxide complex. This was corroborated by QTAIM bcp properties; the Ce–O ρ_{BCP} (0.2563 a.u.) and H_{BCP} (-0.2060 a.u.) values indicate the presence of a Ce–O covalent bond. The triplet state $\text{CeO}(\text{NO}_3)_4^-$ and the open-shell singlet $\text{CeO}(\text{NO}_3)_4^-$ isomer, which have electronic configurations consistent with a Ce(III) ($4f^1$) metal center interacting with a radical oxygen, were found to be more than 100 kJ mol^{-1} higher in energy. In contrast, the Ln–O distances in $\text{LaO}(\text{NO}_3)_3^-$ and $\text{LuO}(\text{NO}_3)_3^-$ are both ~ 0.1 Å longer than the La–OH distance in $\text{La}(\text{OH})(\text{NO}_3)_3^-$,

clearly indicating that these are not Ln=O double bonds, this in accord with the very high IE4 for La and Lu. The $\text{LaO}(\text{NO}_3)_3^-$ and $\text{LuO}(\text{NO}_3)_3^-$ M–O (oxide) topological properties are characteristic of ionic bonds (Table S1, ESI[†]). $\text{LaO}(\text{NO}_3)_3^-$ and $\text{LuO}(\text{NO}_3)_3^-$ are in their doublet ground spin state, and the spin density is localized on the (oxide) oxygen atoms, confirming that the metal electronic configuration is consistent with a Ln(III) central cation interacting with a radical oxygen. The oxidation states of all of the other $\text{LnO}(\text{NO}_3)_3^-$ that hydrolyze with similarly high efficiencies are apparently Ln(III) such that hydrolysis proceeds efficiently. The $\text{PrO}(\text{NO}_3)_3^-$ doublet ground state structure obtained at the level of theory used here (DFT) has a mixed electronic configuration, with a spin density corresponding to 1.5 electrons localized on the metal center, 0.5 electrons of opposite spin localized on the oxygen atom, and a Pr–O oxide bond distance of 1.85 Å. The quartet spin state $\text{Pr}^{\text{III}}\text{O}(\text{NO}_3)_3^-$ isomer that comprises two electrons localized on the metal atom ferromagnetically coupled with a radical oxygen atom was found to be 25 kJ mol^{-1} higher in energy ($d_{\text{Pr-O}} = 2.22$ Å), whereas the antiferromagnetically coupled doublet spin state isomer is 19 kJ mol^{-1} higher in energy ($d_{\text{Pr-O}} = 2.19$ Å) than the GS isomer. The characteristics of the electronic configuration of the $\text{PrO}(\text{NO}_3)_3^-$ ground state and the presence of low-energy isomers suggest that an accurate description of this species could only be obtained using multireference methodologies, and support the hypothesis of $\text{PrO}(\text{NO}_3)_3^-$ having a mixed Ln(IV)/Ln(III) character. Based on the very slow hydrolysis rates for $\text{NdO}(\text{NO}_3)_3^-$ and $\text{TbO}(\text{NO}_3)_3^-$ it is inferred that these are not Ln(III) complexes. The IE4 of Nd and Tb are intermediate between IE4[Ce] and IE4 for those Ln for which the oxidation state in $\text{LnO}(\text{NO}_3)_3^-$ is III. We conclude that $\text{NdO}(\text{NO}_3)_3^-$ and $\text{TbO}(\text{NO}_3)_3^-$, like $\text{PrO}(\text{NO}_3)_3^-$, likely exhibit oxidation states intermediate between Ln(III) and Ln(IV). As remarked above, based on comparison of IE4 for Ce with IE4 for An = Pu, Am and Cm, it is inferred that the oxidation states are An(IV) in the $\text{AnO}(\text{NO}_3)_3^-$ complexes, in accord with the absence of hydrolysis.

The computed structures of $\text{M}(\text{NO}_3)_4^-$, $\text{M}(\text{OH})(\text{NO}_3)_3^-$ and $\text{MO}(\text{NO}_3)_3^-$ for M = Sc and Y are similar to those for M = Ln, with the M–O bond distances paralleling the M^{3+} radii (Fig. 1 and Tables 2 and 3). The structures of the Al complexes are different from the others, as seen in Fig. 1, evidently a result of steric crowding due to the much smaller radius of Al^{3+} . In contrast to the other $\text{M}(\text{NO}_3)_4^-$ with three bidentate nitrate ligands, in the case of $\text{Al}(\text{NO}_3)_4^-$ there are two bidentate and two monodentate nitrates, with the three Al–O distances as given in Table 2. In both $\text{Al}(\text{OH})(\text{NO}_3)_3^-$ and $\text{AlO}(\text{NO}_3)_3^-$ all three nitrates are monodentate with short Al–O distances. The characteristics of the $\text{MO}(\text{NO}_3)_3^-$ ions (M = Al, Sc, and Y) are similar to those of $\text{LnO}(\text{NO}_3)_3^-$ ions for which the oxidation state IV is inaccessible, *i.e.* the M–O distances are longer than the M–OH distances and the spin density is localized on the oxide oxygen atom. In particular, the topological properties of the $\text{MO}(\text{NO}_3)_3^-$ oxides (M = Al, Sc, and Y) are similar to those of $\text{LaO}(\text{NO}_3)_3^-$ and $\text{LuO}(\text{NO}_3)_3^-$ (Table S1, ESI[†]).

Conclusions

Tetranitrate ions, $M^{III}(\text{NO}_3)_4^-$, were produced by ESI and subjected to low-energy CID in QIT mass spectrometers. The dominant CID products for $M = \text{Ce}, \text{Pr}, \text{Nd}, \text{Tb}, \text{Pu}, \text{Am}$ and Cm are the metal oxide ions, $\text{MO}(\text{NO}_3)_3^-$. The main CID product for the rest of the lanthanide ions are $\text{M}(\text{OH})(\text{NO}_3)_3^-$, which are produced in a secondary reaction by hydrolysis of initially formed $\text{MO}(\text{NO}_3)_3^-$. DFT results confirm that in the case of Ce the most stable $\text{CeO}(\text{NO}_3)_3^-$ complex contains a Ce–O covalent bond and a metal electronic configuration consistent with a Ce(IV) oxidation state. In contrast, the $\text{LaO}(\text{NO}_3)_3^-$ and $\text{LuO}(\text{NO}_3)_3^-$ anion complexes contain metal centers in the Ln(III) oxidation state interacting electrostatically with O^- radical ions. The measured hydrolysis rates for $\text{MO}(\text{NO}_3)_3^-$ shows that the ions more resistant to hydrolysis are those containing metals with the relatively low IE4 (and IV/III reduction potentials), *i.e.* the lanthanides Ce, Pr, Tb and Nd, and the actinides Pu, Am and Cm. For $\text{PrO}(\text{NO}_3)_3^-$ the computations suggest that the oxidation state is intermediate Pr(IV/III). Based on the hydrolysis kinetics and the IE4 values, we conclude that Nd and Tb, like Pr, are likely in intermediate Ln(IV/III) oxidation states, whereas Pu, Am and Cm are likely in the An(IV) oxidation states. Among the $\text{LnO}(\text{NO}_3)_3^-$ the oxidation state is Ln(IV) only for Ce. Slow hydrolysis for $\text{AlO}(\text{NO}_3)_3^-$ despite favorable energetics reveals a kinetic hindrance for association of water when the ionic radius of the metal ion is small. The computed energetics of the hydrolysis reactions are in agreement with the experimental results. Besides its relevance for a better comprehension of the gas-phase behavior of lanthanides and actinides, this study may be of use for the interpretation of mass spectra of ligated lanthanide, actinide, and other metal complexes.

Acknowledgements

This work was supported by Fundação para a Ciência e a Tecnologia (PhD grant SFRH/BD/70475/2010 to A.F.L.; RNEM – Rede Nacional de Espectrometria de Massa: C2TN-IST and CQE-IST Nodes; projects PTDC/QUI-QUI/108977/2008 and PEst-OE/QUI/UI0100/2011); European Commission (projects ACSEPT – FP7-Euratom/CP-2007-211267 and ACTINET-III-FP7-III-232631/JRP17). The work of MCM was supported by Università della Calabria. The work of PXR and JKG was fully supported by the U.S. Department of Energy, Office of Basic Energy Sciences, Heavy Element Chemistry, at LBNL under Contract No. DE-AC02-05CH11231. This research used resources of the National Energy Research Scientific Computing Center (NERSC), which is supported by the Office of Science of the U.S. Department of Energy under Contract No. DE-AC02-05CH11231. The work at the CEA was supported by the DISN/RSTB/RBPCH (Basic Research for Physical Chemistry) Program.

References

- 1 NIST Chemistry WebBook, NIST Standard Reference Database Number 69, ed. P. J. Linstrom and W. G. Mallard, National

- Institute of Standards and Technology, Gaithersburg, MD, 2014.
- 2 K. Butkow and W. Tschassowenny, *Acta Physicochim. URSS*, 1936, **5**, 645–650.
- 3 W. W. Wendlandt, *Thermochim. Acta*, 1974, **10**, 101–107.
- 4 J. Mu and D. D. Perlmutter, *Thermochim. Acta*, 1982, **56**, 253–260.
- 5 L. Markov and K. Petrov, *React. Solids*, 1986, **1**, 319–327.
- 6 I. Van Driessche, R. Mouton and S. Hoste, *Mater. Res. Bull.*, 1996, **31**, 979–992.
- 7 S. Dash, M. Kamruddin, S. Bera, P. K. Ajikumar, A. K. Tyagi, S. V. Narasimhan and B. Raj, *J. Nucl. Mater.*, 1999, **264**, 271–282.
- 8 C. K. Ullal, K. R. Balasubramaniam, A. S. Gandhi and V. Jayaram, *Acta Mater.*, 2001, **49**, 2691–2699.
- 9 C. Ehrhardt, M. Gjikaj and W. Brockner, *Thermochim. Acta*, 2005, **432**, 36–40.
- 10 W. Brockner, C. Ehrhardt and M. Gjikaj, *Thermochim. Acta*, 2007, **456**, 64–68.
- 11 R. Karita, H. Kusaba, K. Sasaki and Y. Teraoka, *Catal. Today*, 2007, **126**, 471–475.
- 12 J. R. A. Sietsma, H. Friedrich, A. Broersma, M. Versluijs-Helder, A. J. van Dillen, P. E. de Jongh and K. P. de Jong, *J. Catal.*, 2008, **260**, 227–235.
- 13 E. Marceau, M. Che, J. Cejka and A. Zukal, *ChemCatChem*, 2010, **2**, 413–422.
- 14 D. G. Colombo, D. C. Gilmer, V. G. Young, S. A. Campbell and W. L. Gladfelter, *Chem. Vap. Deposition*, 1998, **4**, 220–222.
- 15 Z. B. Wu, M. Okuya and S. Kaneko, *Thin Solid Films*, 2001, **385**, 109–114.
- 16 W. N. Wang, Y. Itoh, I. W. Lenggoro and K. Okuyama, *Mater. Sci. Eng., B*, 2004, **111**, 69–76.
- 17 J. R. A. Sietsma, J. D. Meeldijk, J. P. den Breejen, M. Versluijs-Helder, A. J. van Dillen, P. E. de Jongh and K. P. de Jong, *Angew. Chem., Int. Ed.*, 2007, **46**, 4547–4549.
- 18 R. Strobel and S. E. Pratsinis, *Phys. Chem. Chem. Phys.*, 2011, **13**, 9246–9252.
- 19 W. W. Wendlandt and J. L. Bear, *J. Inorg. Nucl. Chem.*, 1960, **12**, 276–280.
- 20 M. D. S. Kumar, T. M. Srinivasan, C. Subramanian and P. Ramasamy, *Ceram. Int.*, 1997, **23**, 419–423.
- 21 Nibha, I. P. S. Kapoor, G. Singh and R. Frohlich, *J. Mol. Struct.*, 2013, **1034**, 296–301.
- 22 Nibha, B. P. Baranwal, G. Singh and C. G. Daniliuc, *J. Rare Earths*, 2014, **32**, 545–552.
- 23 S. Dill and H. J. Meyer, *Z. Naturforsch., B: J. Chem. Sci.*, 2006, **61**, 11–16.
- 24 S. Mollah, A. D. Pris, S. K. Johnson, A. B. Gwizdala and R. S. Houk, *Anal. Chem.*, 2000, **72**, 985–991.
- 25 F. M. Li, M. A. Byers and R. S. Houk, *J. Am. Soc. Mass. Spectrom.*, 2003, **14**, 671–679.
- 26 *CRC Handbook of Chemistry and Physics*, ed. D. R. Lide, CRC Press, Boca Raton, Florida, 84th edn, 2003.
- 27 R. Frański, K. Sobieszczuk and B. Gierczyk, *Int. J. Mass Spectrom.*, 2014, **369**, 98–104.

- 28 A. M. Ricks, L. Gagliardi and M. A. Duncan, *J. Phys. Chem. Lett.*, 2011, **2**, 1662–1666.
- 29 W. Huang, W. H. Xu, J. Su, W. H. E. Schwarz and J. Li, *Inorg. Chem.*, 2013, **52**, 14237–14245.
- 30 G. S. Groenewold, J. Oomens, W. A. de Jong, G. L. Gresham, M. E. McIlwain and M. J. Van Stipdonk, *Phys. Chem. Chem. Phys.*, 2008, **10**, 1192–1202.
- 31 J. Oomens, L. Myers, R. Dain, C. Leavitt, V. Pham, G. Gresham, G. Groenewold and M. Van Stipdonk, *Int. J. Mass Spectrom.*, 2008, **273**, 24–30.
- 32 D. Schröder, K. P. de Jong and J. Roithová, *Eur. J. Inorg. Chem.*, 2009, 2121–2128.
- 33 D. Schröder, M. C. Holthausen and H. Schwarz, *J. Phys. Chem. B*, 2004, **108**, 14407–14416.
- 34 L. Berthon, N. Zorz, B. Gannaz, S. Lagrave, T. Retegan, A. Fermvik and C. Ekberg, *IOP Conf. Ser.: Mater. Sci. Eng.*, 2010, **9**, 012059.
- 35 D. Rios, P. X. Rutkowski, D. K. Shuh, T. H. Bray, J. K. Gibson and M. J. Van Stipdonk, *J. Mass Spectrom.*, 2011, **46**, 1247–1254.
- 36 P. X. Rutkowski, M. C. Michelini, T. H. Bray, N. Russo, J. Marçalo and J. K. Gibson, *Theor. Chem. Acc.*, 2011, **129**, 575–592.
- 37 S. Gronert, *J. Am. Soc. Mass Spectrom.*, 1998, **9**, 845–848.
- 38 M. J. Frisch, *et al.*, *Gaussian (revision B01)*, 2009. See ESI† for full citation.
- 39 A. D. Becke, *J. Chem. Phys.*, 1993, **98**, 5648–5652.
- 40 C. T. Lee, W. T. Yang and R. G. Parr, *Phys. Rev. B: Condens. Matter Mater. Phys.*, 1988, **37**, 785–789.
- 41 W. Kuchle, M. Dolg, H. Stoll and H. Preuss, *J. Chem. Phys.*, 1994, **100**, 7535–7542.
- 42 X. Y. Cao, M. Dolg and H. Stoll, *J. Chem. Phys.*, 2003, **118**, 487–496.
- 43 R. Krishnan, J. S. Binkley, R. Seeger and J. A. Pople, *J. Chem. Phys.*, 1980, **72**, 650–654.
- 44 J. P. Blaudeau, M. P. McGrath, L. A. Curtiss and L. Radom, *J. Chem. Phys.*, 1997, **107**, 5016–5021.
- 45 T. Clark, J. Chandrasekhar, G. W. Spitznagel and P. V. Schleyer, *J. Comput. Chem.*, 1983, **4**, 294–301.
- 46 J. G. Norman, P. B. Ryan and L. Noodleman, *J. Am. Chem. Soc.*, 1980, **102**, 4279–4282.
- 47 L. Noodleman, *J. Chem. Phys.*, 1981, **74**, 5737–5743.
- 48 I. Ciofini and C. A. Daul, *Coord. Chem. Rev.*, 2003, **238**, 187–209.
- 49 F. Neese, *Coord. Chem. Rev.*, 2009, **253**, 526–563.
- 50 R. F. W. Bader, *Atoms in Molecules: A Quantum Theory*, Oxford University Press, Oxford, 1990.
- 51 T. A. Keith, *AIMAll (version 13.05.06)*, 2013, aim.tkgristmill.com.
- 52 Y. Gong, H. S. Hu, L. F. Rao, J. Li and J. K. Gibson, *J. Phys. Chem. A*, 2013, **117**, 10544–10550.
- 53 S. G. Bratsch and J. J. Lagowski, *J. Phys. Chem.*, 1985, **89**, 3317–3319.
- 54 S. G. Bratsch and J. J. Lagowski, *J. Phys. Chem.*, 1986, **90**, 307–312.
- 55 R. J. M. Konings, L. R. Morss and J. Fuger, in *The Chemistry of the Actinide and Transactinide Elements*, ed. L. R. Morss, N. M. Edelstein and J. Fuger, Springer, Dordrecht, The Netherlands, 2006, ch. 19, vol. 4, pp. 2113–2224.
- 56 R. D. Shannon and C. T. Prewitt, *Acta Crystallogr., Sect. B: Struct. Crystallogr. Cryst. Chem.*, 1969, **25**, 925–946.